Magnetic, transport and lattice instability behaviour in Co_2NbSn-based systems

2002 J. Phys.: Condens. Matter 14 3775

(http://iopscience.iop.org/0953-8984/14/14/310)

INSTITUTE OF PHYSICS PUBLISHING JOURNAL OF PHYSICS: CONDENSED MATTER

J. Phys.: Condens. Matter **14** (2002) 3775–3793 PII: S0953-8984(02)31963-5

Magnetic, transport and lattice instability behaviour in Co_2NbSn-based systems

C S Garde and J Ray[1]

Low Temperature Physics Group, Tata Institute of Fundamental Research, Homi Bhabha Road, Mumbai 400 005, India

E-mail: jray@tifr.res.in

Received 18 December 2001, in final form 4 March 2002
Published 28 March 2002
Online at stacks.iop.org/JPhysCM/14/3775

Abstract

$Co_2(Nb_{1-x}V_x)Sn$, $Co_2NbSn_{1-y}Ga_y$ and $Co_2NbSn_{1-z}Al_z$ alloy systems exhibit itinerant ferromagnetic behaviour as observed from magnetization and susceptibility studies. Spin fluctuation effects are observed from magnetization, resistivity and thermopower data. The thermal expansion data gave evidence of structural transformation effects due to the formation of a pseudogap in the density of states near the Fermi level.

1. Introduction

Magnetic and structural behaviours of 3d-transition-metal-based itinerant systems are strongly governed by the band structure, the density of states $N(E_F)$ at the Fermi level E_F and the magnetic exchange integral I. The shape and position of the 3d bands and the overlap and hybridization of the different wavefunctions (near E_F) play a crucial role. When I is sufficiently strong, $IN(E_F) \gg 1$, ferromagnetism (F) occurs [1]. The value of $N(E_F)$ depends on the conduction electron density n_0. In the F state, each electron moves in the self-consistent field generated by the other electrons. Consequently, the electron spins are directed along the average field. However, those alloy systems which are at the threshold of non-magnetic to F behaviour are of interest, as their magnetic behaviour is weak [2, 3] and not yet fully understood. The magnetization (M) behaviour is quite complex. Below T_C, M^2 can exhibit either a T^2-law or a $T^{4/3}$-law dependence due to different spin fluctuation (SF) processes [2]. These SF effects can only partially explain all the magnetic and transport behaviour. The presence of a large $N(E_F)$ could also lead to lattice transformation (LT) effects [4] arising from the interaction of band electrons with the crystal fields. Some studies have been carried out on weak magnetic ternary systems such as Co_2TZ (where T = transition element and Z = sp element) systems [4–8]. Several aspects are still not well understood. Most important amongst them are the influence of hybridization (of the Co and T bands) and the role of n_0 (provided by the Z atoms) on the

[1] Author to whom any correspondence should be addressed.

Table 1. Lattice constants and various characteristic structural and magnetic parameters.

System	a (Å)	r_0	T_S (K)	T_C (K)	T_M (K)	$\mu_s(0)$ (μ_B/Co)	θ_p (K)	μ_p (μ_B/Co)
$Co_2(Nb_{1-x}V_x)Sn$								
$x = 0.0$	6.149	0.89	227	109	—	0.40	5	1.10
0.2	6.120	0.84	208	81	—	0.30	20	1.02
0.3	6.092	0.82	203	55	9	0.23	20	0.93
0.5	6.054	0.53	—	80	6	0.25	30	0.94
0.7	6.015	0.56	—	92	—	0.24	20	1.00
1.0	5.958	0.62	—	105	—	0.26	10	1.01
$Co_2NbSn_{1-y}Ga_y$								
$y = 0.1$	6.129	1.0	145	75	—	0.42	45	1.10
0.2	6.109	1.0	43	101	—	0.60	130	0.89
0.3	6.089	1.0	—	150	—	0.65	—	—
$Co_2NbSn_{1-z}Al_z$								
$z = 0.1$	6.127	1.0	167	67	—	0.40	70	0.94
0.2	6.106	1.0	—	89	—	0.46	130	0.93
0.3	6.085	1.0	—	120	—	0.51	—	—

magnetic and structural properties. Co_2NbSn is the only Co-based Heusler system [9,10] which exhibits LT effects due to which it transforms from the cubic ($T > T_S$) to the orthorhombic phase ($T < T_S$). The specific shape and the fine structure in the density of states (at E_F) play a crucial role in the onset of the LT effects. In addition, the system also exhibits F behaviour with $T_C = 109$ K. For this reason, we have studied the $Co_2(Nb_{1-x}V_x)Sn$ system varying the hybridization (between the Co and the Nb–V bands) parameter, whereas the $Co_2NbSn_{1-y}Ga_y$ and $Co_2NbSn_{1-z}Al_z$ systems have been studied varying the n_0-parameter and keeping the hybridization (between Co–Nb bands) parameter fixed. Both of these classes of systems have been examined in detail to investigate their complex magnetic and structural behaviour.

2. Experimental details

All the alloys were prepared in an arc furnace under flowing argon. The buttons were flipped and remelted 3–4 times to ensure homogeneity. The polycrystalline samples were drawn into cylindrical rods by the cold-suction technique. They were annealed at 800 °C for 100 h and then quenched in water. All the systems were found to crystallize in the cubic (Heusler) structure. The lattice parameters a (table 1) for all the systems were found to be close to the reported values [11]. The parameter a varied smoothly (figures 7 and 8) with variation of x, y and z. The magnetization M and dc susceptibility ($\chi = M/H$) were carried out in a SQUID magnetometer (Quantum Devices, USA). H is the applied field. The samples were cooled in zero field as well as external magnetic fields (1 kOe) to measure zero-field-cooled (ZFC) and field-cooled (FC) susceptibilities, respectively. The transport measurements were carried out on the cylindrical (approximately 25 mm in length and 2 mm in diameter) samples. The standard four-probe method was employed for resistivity (ρ) measurements. A dc current of 100 mA was passed through the sample using a constant current source (Hewlett Packard, USA) and the voltage across the sample was measured using a nanovoltmeter (Keithley Instruments, USA). The accuracy of the ρ-measurements is better than 0.01%. For the measurement of the thermopower S and the thermal conductivity λ, AuFe (0.07% Fe) and Cu thermocouple wires were spot welded at the extremities of the sample rod and the voltages were measured

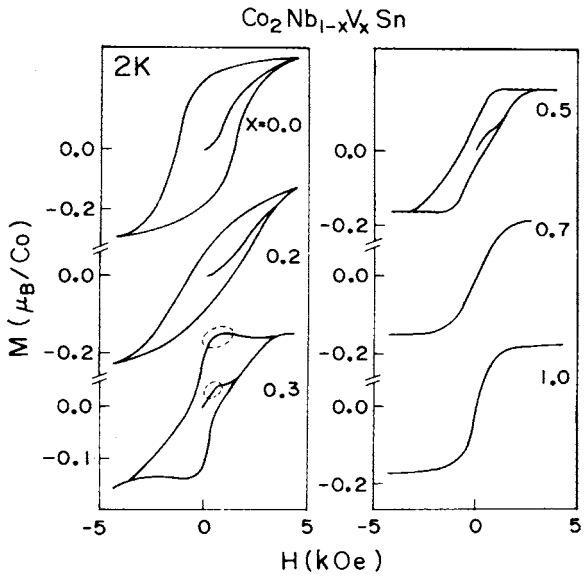

Figure 1. M versus H curves for $Co_2Nb_{1-x}V_xSn$. The details are given in the text.

using a nanovoltmeter (Keithley Instruments, USA) for calculating the temperature gradient ΔT. The accuracies of the S- and λ-measurements are about 5 and 7%, respectively. The thermal expansion $\Delta l/l$ of the samples was measured by a standard parallel-plate capacitance method using a commercial bridge (Andeen Hagerling, USA). l is the length of the sample. The accuracy of $\Delta l/l$ measurements is better than 0.01%.

3. Results

3.1. Magnetization studies

For $x = 0$ and 0.2, the M-curves (at 2 K) exhibit (figure 1) hysteresis behaviour which is typical of F systems. For $x = 0.3$, the curves (around 0.7 kOe) exhibit (for both increasing as well as decreasing H) hump-like features (dashed circles—figure 1). For $x = 0.5$, these hump-like features become less prominent. These humps could arise if a given curve results from a superimposition of two loops (figures 2(a) and (b)). The small loop (figure 2(a)) may arise from ferrimagnetic effects whereas the large loop (figure 2(b)) may arise from ferromagnetic (F) behaviour. Further, the curve (for $x = 0.3$) tends to saturate (figure 1) for $H > 4$ kOe. The plateau in the virgin curve (around 0.7 kOe) could arise due to ferrimagnetic behaviour whereas the saturation behaviour (for $H > 4$ kOe) could be related to F behaviour. At higher temperatures ($T = 10$ K), the curves (for $x = 0.3$ and 0.5) do not exhibit (figure 3) the hump-like feature but rather display simple hysteresis loops corresponding to F order only. The curves (for $x = 0.7$ and 1), exhibit (figure 1) a sharp rise (and a tendency to saturate at higher fields) indicating F behaviour. However, they do not develop hysteresis behaviour. The absence of the hysteresis behaviour could indicate that the magnetic interactions are isotropic [12]. For all y and z, the curves (at $T = 2$ K), exhibit (figure 4) hysteresis and saturation behaviour suggesting the occurrence of F behaviour.

The M^2 versus H/M curves (Arrott plots—figures 5 and 6) exhibit a linear behaviour (for large $H/M > 100$ kOe/μ_B). This linear behaviour is typical of Arrott plots [13]. The extrap-

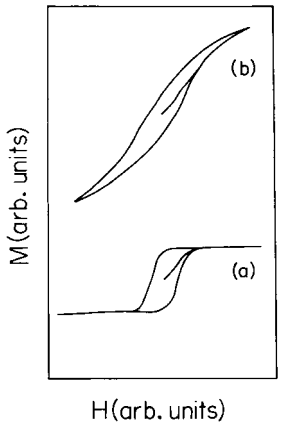

Figure 2. M versus H curve. The details are given in the text.

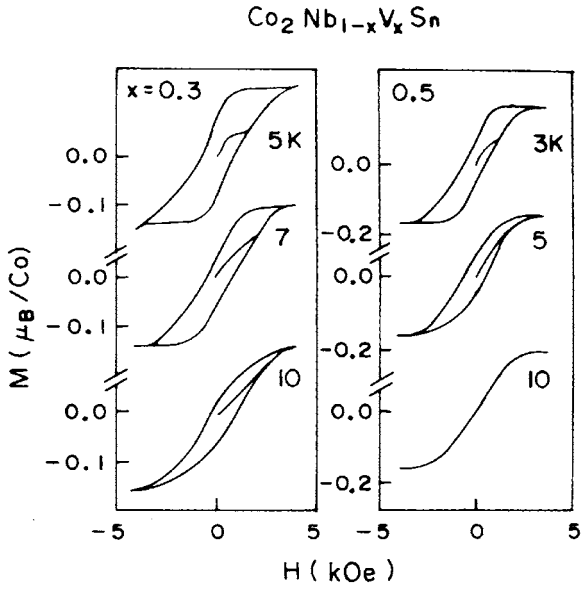

Figure 3. M versus H curves for $Co_2Nb_{1-x}V_xSn$.

olation (dashed line—figures 5 and 6) of the linear portion of the curve to $H/M = 0$ (at 2 K) gives a positive value which corresponds to the spontaneous magnetization $\mu_s(0)$ per Co atom (table 1). This positive value (at higher temperatures) of the spontaneous magnetization μ_s (figures 5 and 6) confirms F behaviour. The temperature at which the Arrott curve (figures 5 and 6) passes through the origin (i.e. $\mu_s = 0$) is defined as the Curie temperature T_C. With increase of x, y and z (up to $x \leqslant 0.3$, $y \leqslant 0.1$ and $z \leqslant 0.1$), the value of T_C decreases initially and then increases (for higher values of x, y and z) exhibiting a minimum (figures 7 and 8) behaviour. This minimum behaviour is not understood. We note that the existence of the linear part of the Arrott plots (figures 5 and 6) is in accordance with the Stoner–Wohlfarth (SW) model [1] for itinerant electrons. Within this model [1], the value of T_C is given by $T_C^2 = T_F^2(IN(E_F) - 1)$. T_F is the bandwidth. The other symbols have been defined earlier. However (at low values of

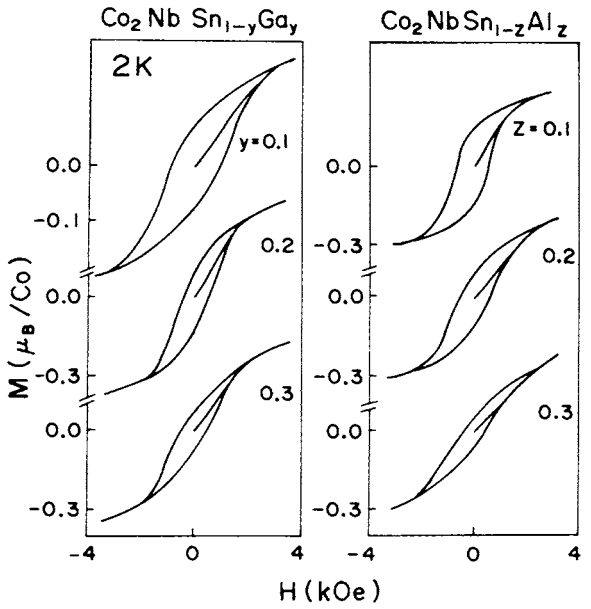

Figure 4. M versus H curves for $Co_2NbSn_{1-y}Ga_y$ and $Co_2NbSn_{1-z}Al_z$.

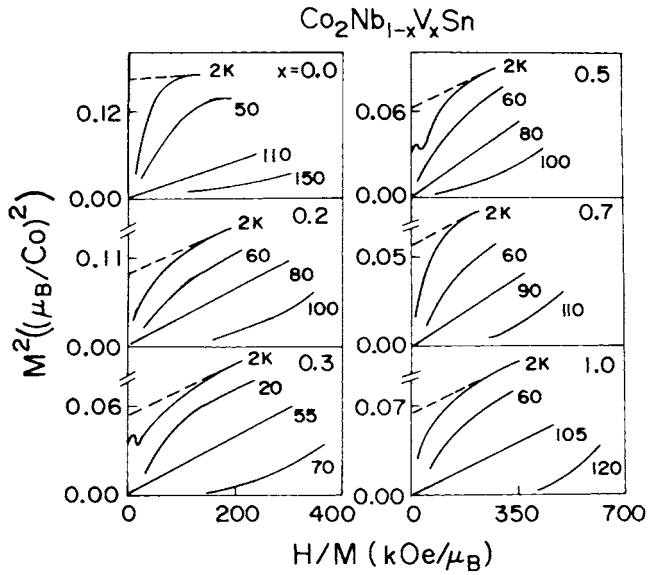

Figure 5. M^2 versus H/M curves for $Co_2Nb_{1-x}V_xSn$. The details are given in the text.

$H/M < 100\,\mathrm{kOe}/\mu_B$), deviations (dashed curves—figures 5 and 6) from this linear behaviour cannot be explained within this model. This could happen if SF effects (which are not taken into consideration in the SW model) are present. They influence the low-temperature ($T < T_C$) M-behaviour significantly. Such SF effects have been observed earlier in the Ni_3Al system [2]. We note that the low-field ($H \leqslant 5\,\mathrm{kOe}$) magnetization values (figure 1) correspond to the initial portion of the Arrott plots ($H/M \ll 100\,\mathrm{kOe}/\mu_B$—figure 5) where μ_s depends strongly on

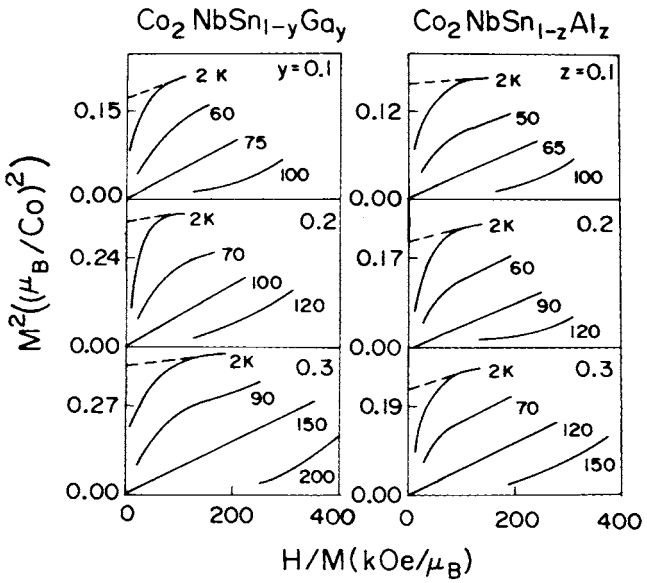

Figure 6. M^2 verses H/M curves for $Co_2NbSn_{1-y}Ga_y$ and $Co_2NbSn_{1-z}Al_z$. The details are given in the text.

H, whereas in the framework of both the SW and the SF models [1,2], the μ_s-values can only be correctly estimated from the curves which are roughly parallel to the $T = T_C$ graph (in the Arrott plots). However, in our case (figures 5 and 6), such parallel curves (over the entire field range at different temperatures) were not observed. Hence, in the first approximation, μ_s was estimated by extrapolating (to $H/M = 0$) their high-field saturated value (figures 5 and 6). The μ_s^2 versus r^2 ($r = T/T_C$) graphs are found to be linear (figure 9(a)) only over a limited temperature range ($r < r_0$). At $r = r_0$, departures (dashed curves—figure 9) from linearity occur. For $r > r_0$, μ_s^2 varies as $T^{4/3}$ (figure 9(b)) instead of T^2. The T^2-dependence [2] arises due to single-particle spin-flip-like fluctuations (first process), whereas the $T^{4/3}$-dependence [2] arises due to modified fluctuations (second process) arising from many-body effects and increased itineracy. In the F state ($T \ll T_C$), the electron spins are directed along the average field direction and the first process is important, whereas, as the temperature is progressively increased (up to T_C), the second process becomes important. This second process could occur if the Co d band gets partially delocalized due to overlap with the Nb (or V) band and E_F lies in that overlapped region. This could enhance the itinerant character of the electrons. For $0 \leqslant x \leqslant 0.3$, we have $r_0 \sim 0.9$ (table 1), whereas for $0.5 \leqslant x \leqslant 1.0$, $r_0 \sim 0.6$. The decrease in the r_0-values (with increase in x—table 1) indicates strengthening of the second process. In contrast, by varying y and z, we observe that the graphs are linear (figure 10) over the entire temperature range ($r_0 = 1$—table 1) and hence only the first process is important here.

3.2. Susceptibility studies

For $Co_2(Nb_{1-x}V_x)Sn$ ($0 \leqslant x \leqslant 0.3$), the χ-values (with lowering of T) of the FC curve increase smoothly (continuous curve—figure 11) and saturate at the lowest temperature. The point of inflection is found to be close to the value of T_C (arrows—figure 11) obtained from the Arrott plots. For $0.5 \leqslant x \leqslant 1$, the FC curves (continuous curve—figure 11) exhibit a sudden change in slope near T_C (arrow—figure 11). As the temperature is further lowered (for $x = 0.3$

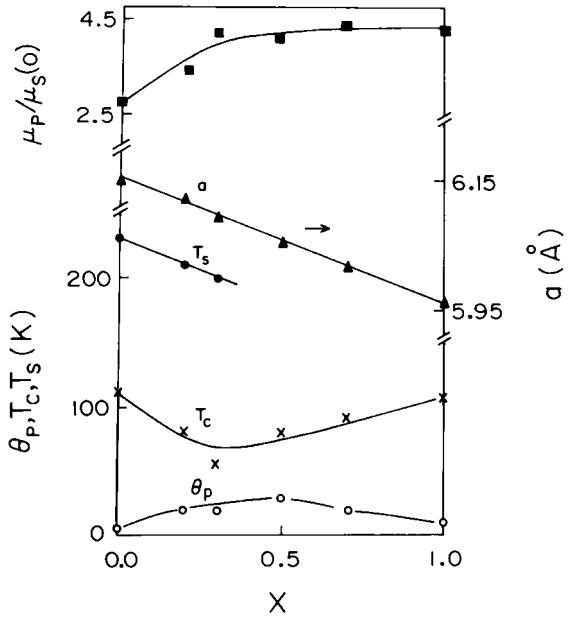

Figure 7. Curves for θ_p, T_C, T_S, a and $\mu_p/\mu_s(0)$ for $Co_2Nb_{1-x}V_xSn$. Various symbols associated with different parameters are shown. The continuous curves are hand drawn to guide the eye. The horizontal arrow denotes the appropriate y-axis for a.

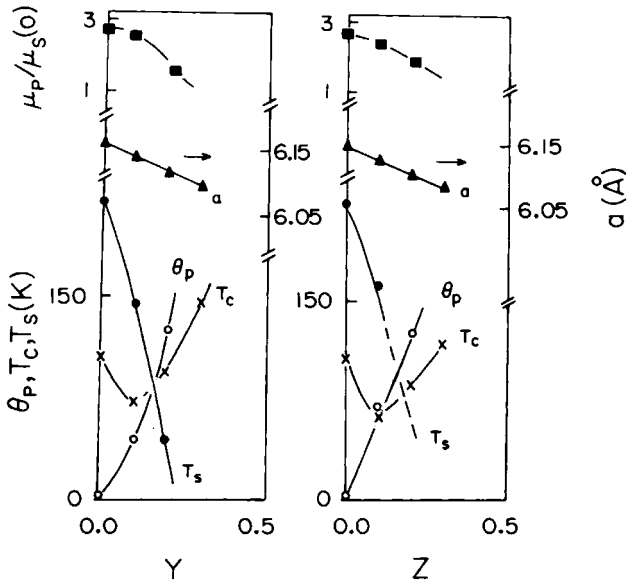

Figure 8. Curves for θ_p, T_C, T_S, a and $\mu_p/\mu_s(0)$ for $Co_2NbSn_{1-y}Ga_y$ and $Co_2NbSn_{1-z}Al_z$. Various symbols associated with different parameters are shown in the figure. The continuous curves are hand drawn to guide the eye. The horizontal arrow denotes the appropriate y-axis for a.

and 0.5), the FC curves (continuous curve—figure 12) exhibit a peak (arrow—figure 12) at the (respective) characteristic temperatures $T_M = 9$ and 6 K (table 1). This could be related

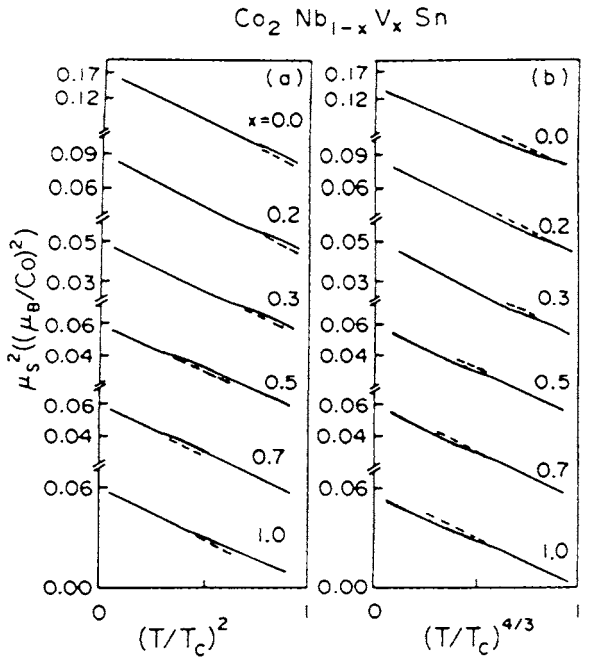

Figure 9. (*a*) μ_s^2 versus $(T/T_C)^2$ and (*b*) μ_s^2 versus $(T/T_C)^{4/3}$ curves for $Co_2Nb_{1-x}V_xSn$.

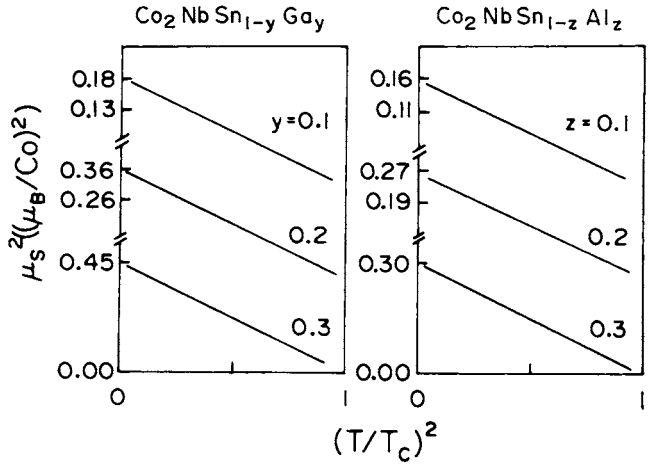

Figure 10. μ_s^2 versus $(T/T_C)^2$ curves for $Co_2NbSn_{1-y}Ga_y$ and $Co_2NbSn_{1-z}Al_z$.

to complex spin re-ordering effects. These effects could arise if the magnetic sublattices have different types of spin ordering. At still lower temperatures ($T < T_M$), the FC curve goes through a minimum and then increases again.

The ZFC curves (for $x = 0$ and 0.2 and $T < T_C$) lie lower (dashed curve—figure 11) than the FC curves. The ZFC curves (for $x = 0.3$ and 0.5) are identical (figures 11 and 12) with the FC curves (down to $T = T_M$), below which the ZFC curves drop sharply. A similar behaviour has also been observed earlier in other systems like $Cu_2(Mn_vTi_{1-v})Al$ [14]. For

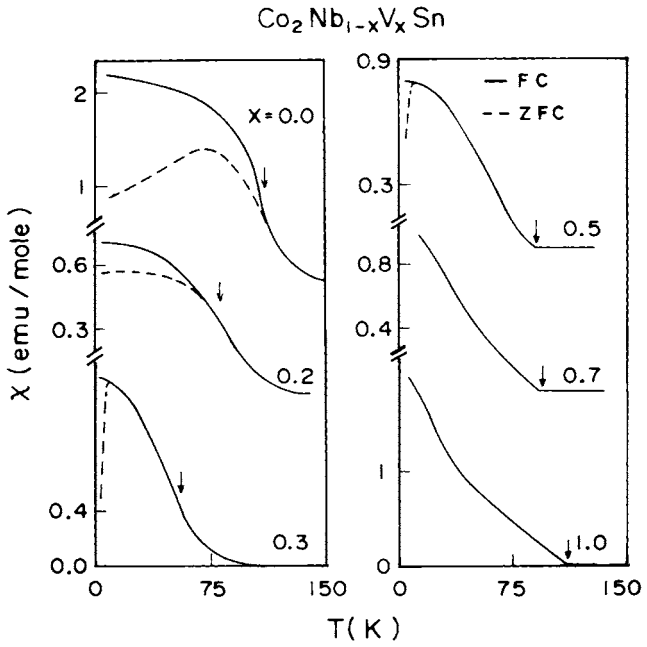

Figure 11. χ versus T curves for $Co_2Nb_{1-x}V_xSn$. The dashed and the continuous curves correspond to ZFC and FC curves, respectively. The arrows indicate T_C.

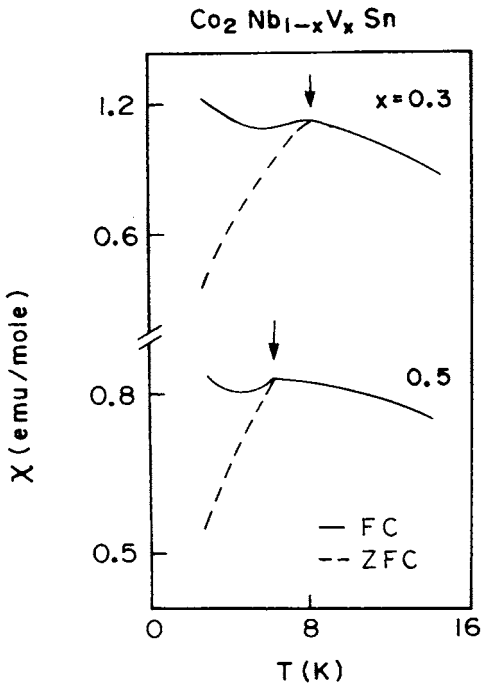

Figure 12. χ versus T curves for $Co_2Nb_{1-x}V_xSn$. The dashed and the continuous curves correspond to ZFC and FC curves, respectively. The arrows indicate T_M.

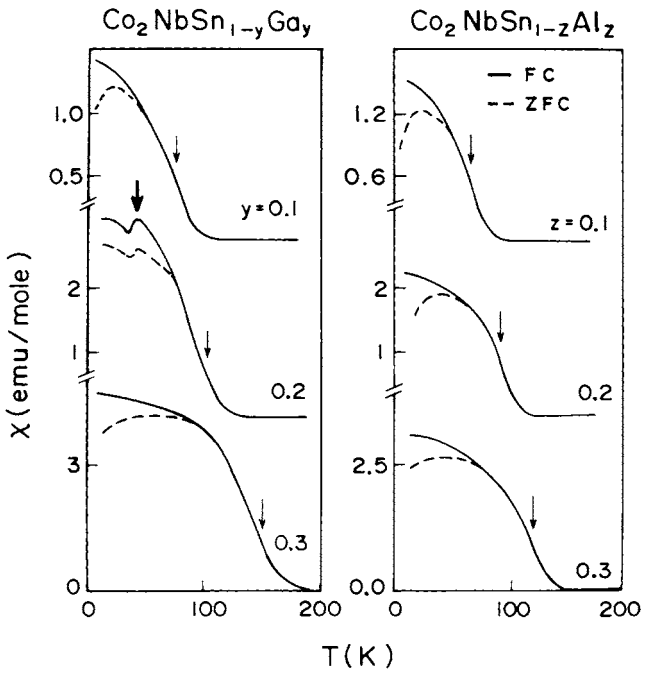

Figure 13. χ versus T curves for $Co_2NbSn_{1-y}Ga_y$ and $Co_2NbSn_{1-z}Al_z$. The dashed and the continuous curves correspond to ZFC and FC curves, respectively. The thin and the thick arrows denote T_C and T_S, respectively.

$x = 0.7$ and 1, the ZFC and FC curves are identical down to 2 K. We note that a complete overlap of the FC and ZFC curves occurs (for $x \geqslant 0.7$) only when the M-curves (figure 1) do not exhibit hysteresis.

For all y and z, the FC curve increases rapidly (continuous curves—figure 13) with decrease of T, indicating the onset of F order. Here also, the value of T_C (thin arrow—figure 13) obtained from the M-data (section 3.1) lies quite close to the point of inflection (figure 13). The FC curve tends to saturate at the lowest temperature ($T = 2$ K). For $y = 0.2$, both the FC and ZFC curves exhibit a kink (thick arrow—figure 13) around 43 K. This kink is not due to any magnetic transition, as our M-studies (section 3.1) did not reveal any magnetic transition around 43 K. We show later (section 3.3) that this feature actually arises at the characteristic temperature T_S due to LT effects. For all x, y and z, the difference between FC and ZFC curves can be understood as follows. For F systems ($T < T_C$), two competing effects [15] come into play. Firstly, the thermal disorder in the spin system decreases with the lowering of temperature and thereby increases χ. Secondly, the movement of domain walls also slows down which results in decrease in χ thereby lowering the ZFC curves (below the FC curves). Further, the competition between the above two processes leads to a maximum (figure 13). The FC curves are found to increase monotonically with decrease in temperature and finally saturate around $T \to 0$. This indicates the absence of domain wall effects. Such an absence is related with the fact that (at T_C) the minimum field required to move the domain walls tends to zero. Therefore, even a small field causes domain wall movements leading to a single-domain feature. Hence for the FC case, the χ-value saturates (for $T \ll T_C$) and corresponds to the single-domain value. For the F system, the domain wall formation and its movement across the sample, on application of field, are governed by the magnetic anisotropy and the pinning centres [12].

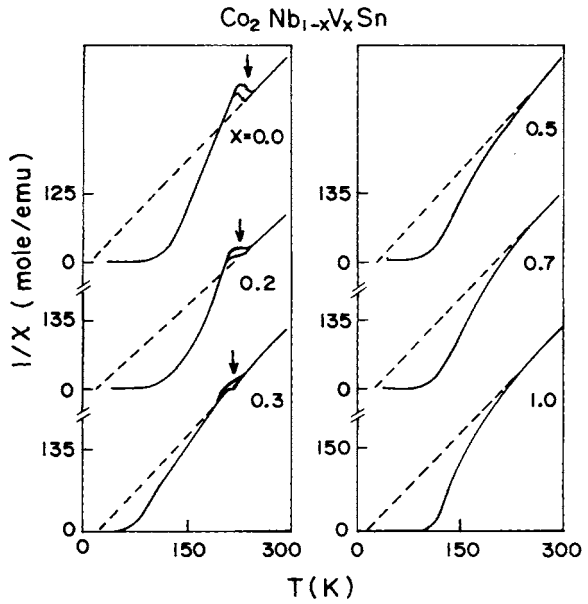

Figure 14. χ^{-1} versus T curves for $Co_2Nb_{1-x}V_xSn$. The arrow denotes T_S. The dashed line is the extrapolation of the linear behaviour observed at high temperatures.

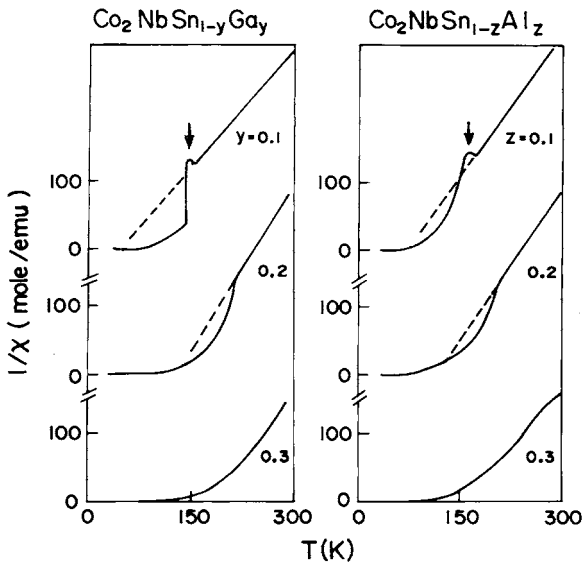

Figure 15. χ^{-1} versus T curves for $Co_2NbSn_{1-y}Ga_y$ and $Co_2NbSn_{1-z}Al_z$. The arrow denotes T_S. The dashed line is the extrapolation of the linear behaviour observed at high temperatures.

The $1/\chi$ curves exhibit a linear behaviour (figures 14 and 15) for $T > 250$ K. This linear portion of the curve can be fitted to the Curie–Weiss law $1/\chi = 3k_B(T - \theta_p)/A\mu_{eff}^2$, where A is Avogadro's number, k_B is the Boltzmann constant, μ_{eff} is the effective magnetic moment and θ_p is the paramagnetic Curie temperature [16]. Paramagnetic moment μ_p is defined as $\mu_{eff} = (\mu_p(\mu_p + 1))^{1/2}$. The variation of θ_p with x (figure 7, table 1) exhibits a maximum

behaviour (figure 7). For $0 \leqslant x \leqslant 1$, we also observed that $\theta_p < T_C$ (table 1—figure 7). This small value of θ_p also implies that SF effects are present, as discussed earlier (section 3.1). Further, $\mu_p/\mu_s(0) \sim 2.7$ (for $x = 0$) increases (figure 7) to 4.2 (for $x = 1$). Weak itinerant ferromagnets [17] are characterized by a low saturation moment per transition metal atom ($\mu_p/\mu_s(0) \gg 1$) compared to strong F metals like Fe or Co ($\mu_p/\mu_s(0) \approx 1$). However, for our systems ($0 \leqslant x \leqslant 1$), $\mu_p/\mu_s(0) > 1$. Hence they can be labelled as weak itinerant systems. With increase in x, the value of $\mu_p/\mu_s(0)$ increased (figure 7) indicating that the itinerant nature became enhanced. This could happen due to an increased overlap between Co–V 3d bands and E_F occurring near the overlapped region. These conclusions are in qualitative agreement with those obtained from our M-studies (section 3.1). In contrast, with increase in y and z, the value of $\mu_p/\mu_s(0)$ decreased (figure 8), indicating a relative weakening of the itinerant behaviour. However, by increasing y and z, the θ_p-value gets enhanced (table 1).

For $0 \leqslant x \leqslant 0.3$, the $1/\chi$ curves exhibit (for $T > 200$ K) thermal hysteresis effects (figure 14). This feature cannot be due to a magnetic transition such as occurs in the paramagnetic regime. The magnetic transition occurs at a lower temperature as evidenced from our M-data (section 3.1). Therefore, this behaviour indicates the onset of the LT effects as also confirmed by our thermal expansion data (section 3.3). The hysteresis loop contains both a minimum and a maximum feature. The mid-point of the loop corresponds to T_S. For $x = 0$, 0.2 and 0.3, the T_S-values (arrows—figure 14) occur around 227, 208 and 203 K, respectively (table 1). However, for $x > 0.3$, no such signature for the LT effect is observed. Further, for $y = 0.1$, the curve exhibits a sharp minimum–maximum behaviour around $T_S = 145$ K (figure 15—table 1). For $y = 0.2$, no such anomaly was observed (figure 15). For $z = 0.1$, the anomaly occurs around $T_S = 167$ K (figure 15, table 1). These anomalous features are clearly associated with LT effects, as also evidenced by our thermal expansion data (section 3.3). However, no thermal hysteresis is observed (around T_S) on varying either y or z.

3.3. Thermal expansion studies

The $\Delta l/l$ curves exhibit a negative minimum quite close to the T_C-values as determined (thin arrows—figures 16 and 17) from our M-data. For $x = 0$, 0.2, 0.3, $y = 0.1$ and $z = 0.1$, the curves also exhibit hysteresis behaviour. This is due to LT effects. The mid-point (thick arrow—figure 16) of the hysteresis loop corresponds to T_S (table 1). For $x > 0.3$, no such hysteresis (or a sharp minimum–maximum) behaviour is observed (figure 16), indicating the absence of LT effects. We note that a typical contribution [17, 18] (to $\Delta l/l$), at any given temperature ($T < T_C$), is the sum total of the electronic, phonon and magnetic contributions. The phonon term varies due to changes in the vibrational modes arising from changes in crystal structure, whereas the electronic term varies due to changes in $N(E_F)$. Our data (for $T < T_C$) reveal that the $\Delta l/l$ values are negative. The magnetic term varied smoothly and became positive (figures 16 and 17) at higher temperatures ($T > T_C$). We note that the magnetic contribution did not change abruptly near T_C.

We now provide a qualitative argument for the occurrence of T_S. For the high-temperature ($T > T_S$) cubic phase, the 3d band could manifest as a single peak (figure 18(a)) in the density of states (DOS), whereas for the low-temperature ($T < T_S$) non-cubic orthorhombic phase, this band could partially split and exhibit a minimum or a pseudogap (figure 18(b)). Such a feature (in the DOS) is also predicted from band-structure calculations [10]. This minimum could occur to the right-hand side of the peak in the DOS. If the Fermi level E_F lies near this minimum (E_1—figure 18(b)), then this could lead to a decrease in the sum of the energies of the occupied states (below E_F) compared to the cubic phase causing LT effects. With increase in y and z, n_0 decreases and hence E_F would move to lower values (E_2 and E_3—figure 18(b)) towards

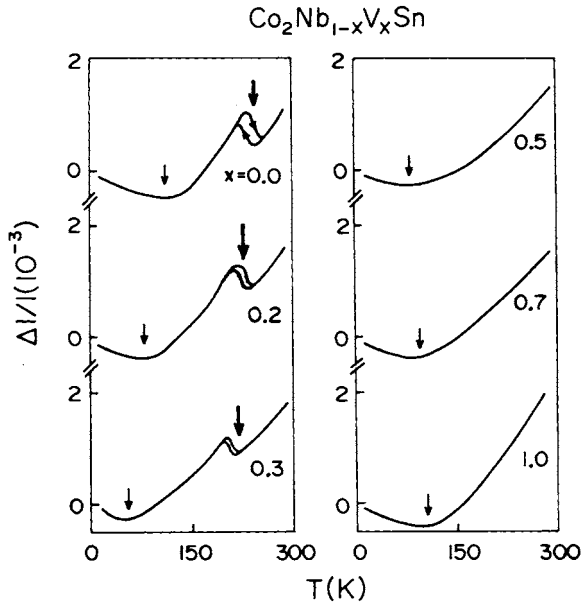

Figure 16. $\Delta l/l$ versus T curves for $Co_2Nb_{1-x}V_xSn$. The thin arrows correspond to T_C-values determined from M-data. The thick arrows denote T_S from $\Delta l/l$ data.

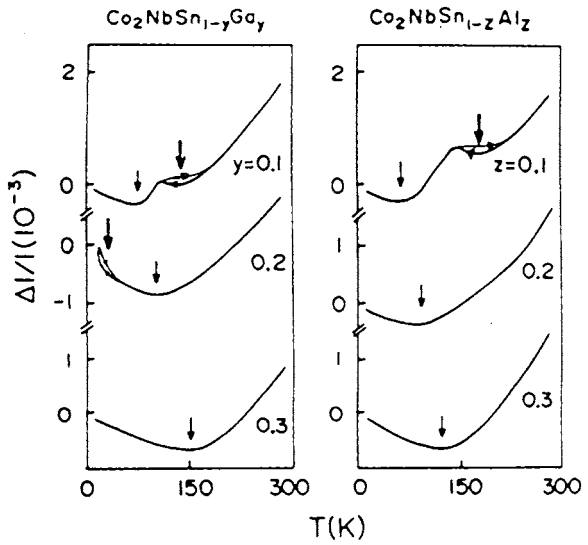

Figure 17. $\Delta l/l$ versus T curves for $Co_2NbSn_{1-y}Ga_y$ and $Co_2NbSn_{1-z}Al_z$. The thin and the thick arrows denote T_C- and T_S-values determined from data for M and $\Delta l/l$ respectively.

the peak. As the E_F moves away from the minimum in the DOS for the orthorhombic phase, the energy difference between the cubic and orthorhombic phase decreases. Consequently, the LT effects get weakened. Hence T_S decreases rapidly (table 1) and finally goes to zero (for $y = 0.3$ and $z = 0.2$). On the other hand, T_S varies only marginally with increasing x (table 1). This is because n_0 (and hence E_F) varies slowly (as the number of valence electrons do not change on increasing x), as both Nb and V occur in the same group of the periodic table.

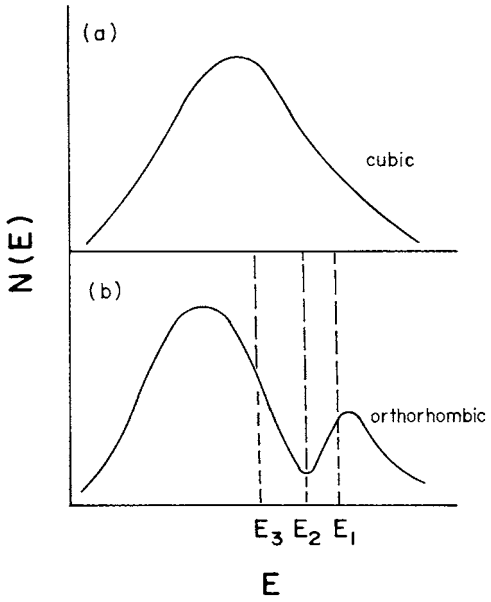

Figure 18. The $N(E)$ versus E curve.

3.4. Resistivity studies

For $0 \leqslant x \leqslant 0.3$, the curves exhibit thermal hysteresis behaviour (figure 19) due to LT effects. The values of T_S (thick arrows—mid-points of the hysteresis loops—figure 19) are close to those obtained from our $\Delta l/l$ data. However, for $x > 0.3$, these LT effects are not observed. Further, the curves do not exhibit any specific signature at T_C. The thin arrows (figure 19) denote the T_C-values as determined from our M-data. For $x = 0$, the curve exhibits an S-shaped behaviour (figure 19) and a tendency to saturate (for $T \leqslant T_S$). Such a behaviour could occur due to SF effects arising from the hybridization of the d bands of Co and Nb. Earlier studies [19] on weak ferromagnets indeed predict such behaviour. This conclusion is also supported by our M-studies (section 3.1). For $x \geqslant 0.3$, the curves exhibit a minimum (around $T = 100$ K), below which they exhibit negative slopes (i.e. an increase of ρ—figure 19) displaying semiconductor-like behaviour. The residual resistivities are calculated to be around 180–200 $\mu\Omega$ cm. We note that Kondo effect cannot manifest here as these are 3d-based concentrated magnetic alloy systems. A similar semiconductor-like behaviour has been observed in other systems like Fe_2VAl [20].

For $y = 0.1$, 0.2 and $z = 0.1$, the curves give evidence for LT effects in the form of a change in slope and a sharp jump (thick arrows—figure 20). These thick arrows denote T_S-values which are close to those determined from our $\Delta l/l$ data. However, no thermal hysteresis effects are observed near T_S. For $y = 0.2$, T_S occurs close to the low-T minimum (around 43 K). The thin arrows (figure 20) denote the T_C-values as determined from our M-data. For $y, z \leqslant 0.3$ also; the curves do not exhibit any signature at T_C and exhibit a tendency to saturate at high temperatures ($T > 200$ K).

3.5. Thermopower studies

The S-curves (figures 21 and 22) are found to be negative over the entire temperature range ($5 < T < 300$ K). The curves do not exhibit any anomaly at T_C. The thin arrows (figures 21

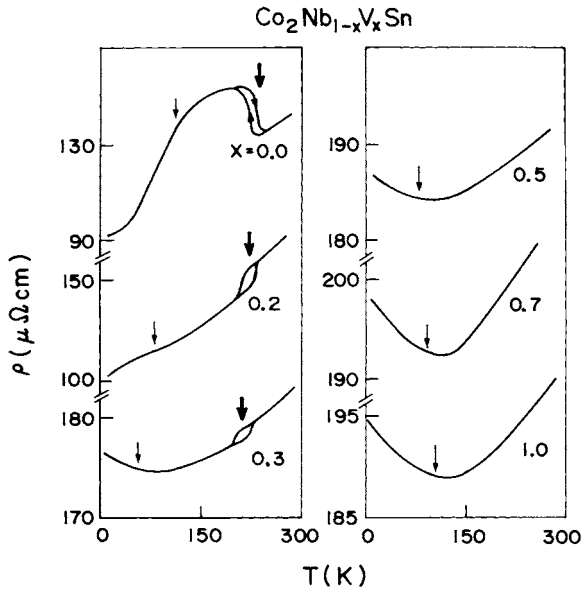

Figure 19. ρ versus T curves for $Co_2Nb_{1-x}V_xSn$. The thin and the thick arrows denote T_C- and T_S-values determined from data for M and $\Delta l/l$ respectively.

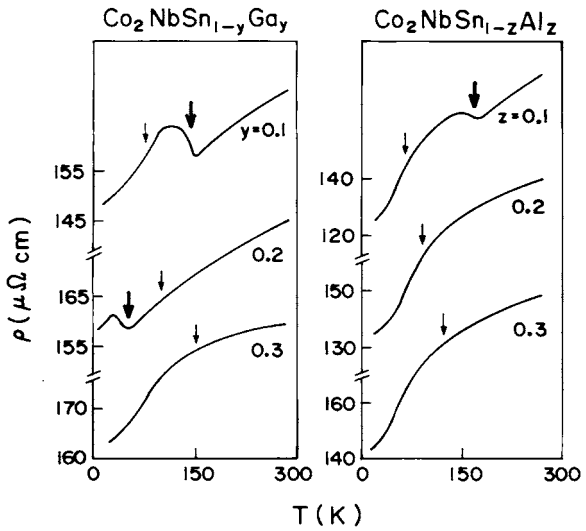

Figure 20. ρ versus T curves for $Co_2NbSn_{1-y}Ga_y$ and $Co_2NbSn_{1-z}Al_z$. The thin and the thick arrows denote T_C- and T_S-values determined from data for M and $\Delta l/l$ respectively.

and 22) denote T_C-values as determined from our magnetic studies. For $x = 0$, 0.2, 0.3, $y = 0.1$, 0.2 and $z = 0.2$, the curves exhibit either a hysteresis or a maximum behaviour (thick arrows—figures 21 and 22) at roughly the same temperature T_S as determined from our $\Delta l/l$ data. However, on varying y or z, no such thermal hysteresis behaviour is observed in contrast to the case for our $\Delta l/l$ data (figure 17). For all the systems, the curves exhibit a linear behaviour at high temperatures ($T > 250$ K) and the values (obtained by extrapolating

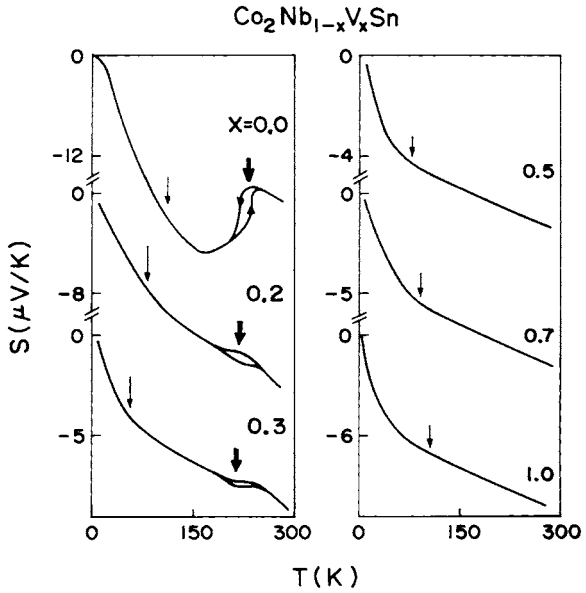

Figure 21. S versus T curves for $Co_2Nb_{1-x}V_xSn$. The thin and the thick arrows denote T_C- and T_S-values determined from data for M and $\Delta l/l$ respectively.

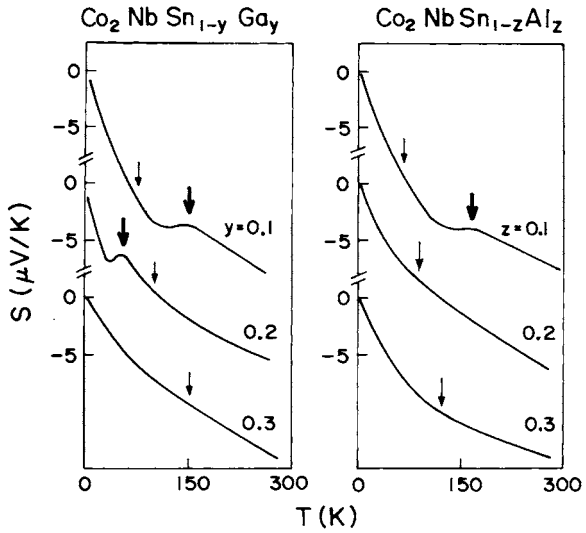

Figure 22. S versus T curves for $Co_2NbSn_{1-y}Ga_y$ and $Co_2NbSn_{1-z}Al_z$. The thin and the thick arrows denote T_C- and T_S-values determined from data for M and $\Delta l/l$ respectively.

the linear behaviour to $T \rightarrow 0$) are non-zero. These non-zero S-values indicate departures from the free-electron behaviour [21, 22], presumably due to SF effects. This conclusion is also supported by our M-studies (section 3.1).

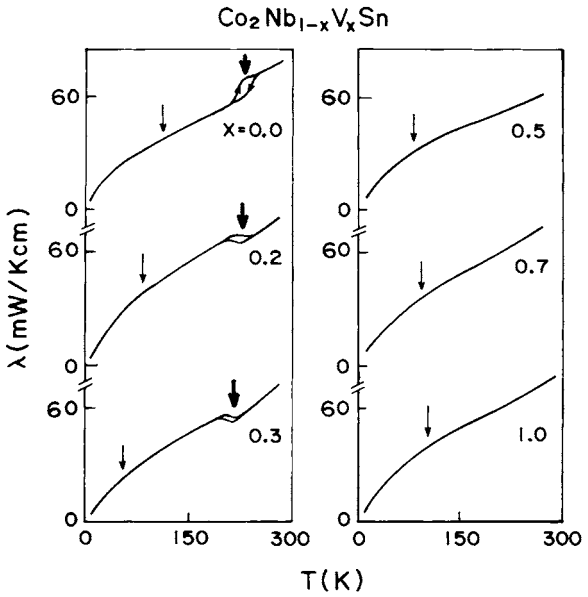

Figure 23. λ versus T curves for $Co_2Nb_{1-x}V_xSn$. The thin and the thick arrows denote T_C- and T_S-values determined from data for M and $\Delta l/l$ respectively.

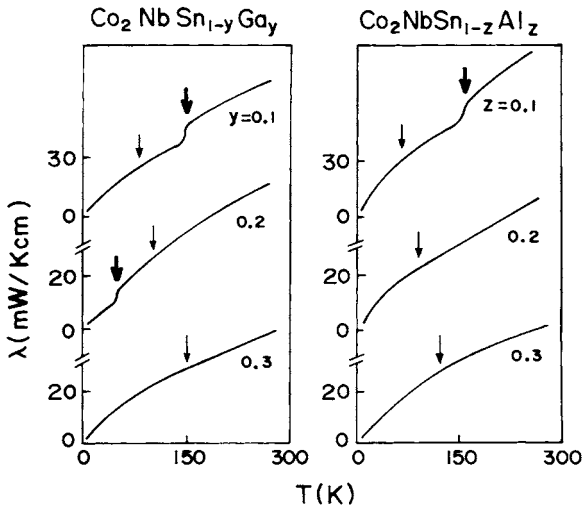

Figure 24. λ versus T curves for $Co_2NbSn_{1-y}Ga_y$ and $Co_2NbSn_{1-z}Al_z$. The thin and the thick arrows denote T_C- and T_S-values determined from data for M and $\Delta l/l$ respectively.

3.6. Thermal conductivity studies

Some of the curves exhibit a sudden change in slope or a hysteresis behaviour (thick arrows—figures 23 and 24) indicating occurrence of LT effects. These thick arrows are close to the T_S-values as calculated from our $\Delta l/l$ studies. However, no anomaly is observed at T_C (thin arrows—figures 23 and 24) as determined from our magnetic studies. The λ-behaviour [22] arises due to the combined influence of electronic (λ_e), phononic (λ_p) and magnetic (λ_m) terms.

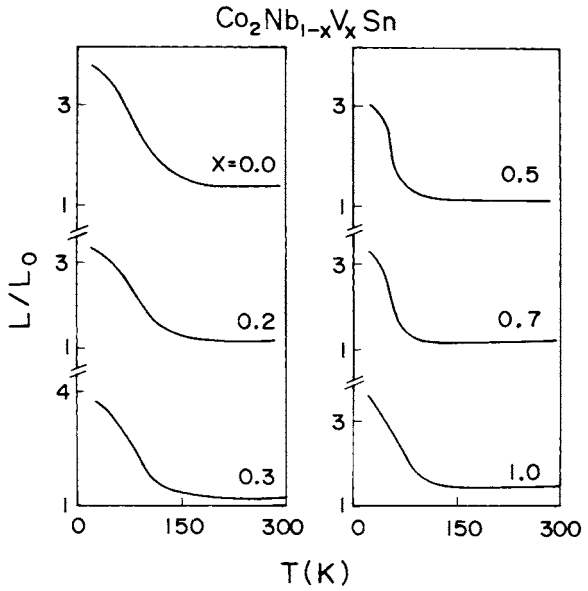

Figure 25. L/L_0 versus T curves for $Co_2Nb_{1-x}V_xSn$.

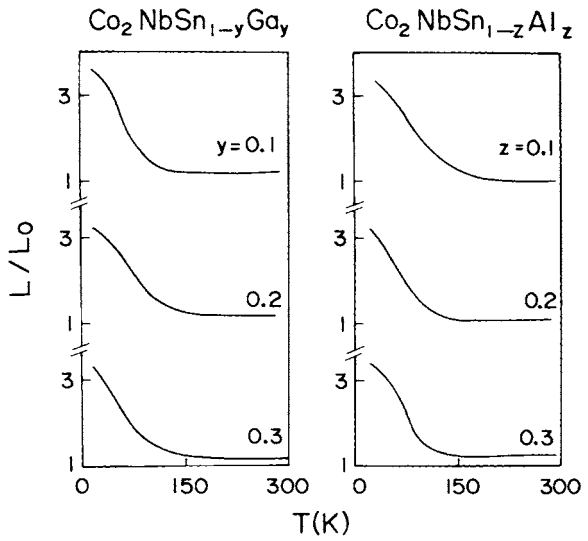

Figure 26. L/L_0 versus T curves for $Co_2NbSn_{1-y}Ga_y$ and $Co_2NbSn_{1-z}Al_z$.

Therefore, the total λ at a given temperature is $\lambda(T) = \lambda_e(T)+\lambda_p(T) + \lambda_m(T)$. The result of the interplay of the above three terms is reflected (figures 25 and 26) in the temperature dependence of the Lorentz number $L = \rho(T)\lambda(T)/T$. In the free-electron picture, L arises only from the λ_e-term and is temperature independent. Its value is given by $L_0 = 2.45 \times 10^{-8}$ WΩ K^{-1}. Our data reveal that L is temperature dependent (figures 25 and 26) and greater than L_0. Therefore the free-electron picture is not valid. Such a deviation from L_0 also indicates that the contribution from λ_p is important. L/L_0 shows a rapid decrease as the temperature is increased beyond 100 K. This happens due to decrease in λ_p as the phonon anharmonic

interaction increases around this temperature. Only at high temperatures ($T > 100$ K) does L/L_0 become temperature independent.

4. Conclusions

Both the F and LT effects arise due to the 3d band of Co in these systems. Co_2NbSn-based systems are found to exhibit a weak itinerant F behaviour as deduced from our χ-studies. For all values of x, μ_s^2 crosses over from a $T^{4/3}$- to T^2-law behaviour as the temperature is gradually lowered below T_C, whereas, on varying both y and z, only a T^2-behaviour has been observed. The T^2-behaviour could arise due to the fluctuation effects from the Co d band, whereas the $T^{4/3}$-behaviour could arise due to the modified fluctuation effects arising from the hybridization of the Co and the Nb–V bands and changes in the position of E_F on varying n_0. Such SF effects are evidenced from our ρ- and S-studies also. Variation of x, y and z induces large changes in the values of both T_C and T_S. With variation of x, y and z, T_C goes through a minimum whereas T_S decreases monotonically. The T_S-variation can be understood in terms of variation of the E_F-value (with respect to x, y and z) and formation of a pseudogap in the DOS.

Acknowledgment

We thank K V Gopalakrishnan for his help in carrying out the SQUID measurements.

References

[1] Rhodes P R and Wohlfarth E P 1963 *Proc. R. Soc.* **273** 247
[2] Mishra S G 1990 *Mod. Phys. Lett.* B **4** 83
[3] Booth J G 1988 *Ferromagnetic Materials* vol 4, ed E P Wohlfarth and K H J Buschow (Amsterdam: North-Holland) p 211
[4] Skriver H L 1985 *Phys. Rev.* B **31** 1909
[5] Van Engen P G and Buschow K H J 1983 *J. Magn. Magn. Mater.* **30** 374
[6] Carbonari A W, Saxena R N, Pendl W Jr, Filho J M, Attili R N, Olzon-Dionysio M and de Souza S D 1996 *J. Magn. Magn. Mater.* **163** 313
[7] Buschow K H J and Van Engen P G 1981 *J. Magn. Magn. Mater.* **25** 90
[8] Miedema A R, de Boer F R and de Chatel P F 1973 *J. Phys. F: Met. Phys.* **3** 1558
[9] Endo K, Ooiwa K and Shinogi A 1992 *J. Magn. Magn. Mater.* **104–7** 2013
[10] Fuji S, Ishida S and Asano S 1989 *J. Phys. Soc. Japan* **58** 3657
[11] *Pearson's Handbook of Crystallographic Data for Intermetallic Phases* 1985 ed P Villars and L D Calvert (Metals Park, OH: American Society for Metals)
[12] Kittel C 1986 *Introduction to Solid State Physics* (New Delhi: Wiley Eastern) p 491
[13] Arrott A and Noakes J E 1967 *Phys. Rev. Lett.* **19** 786
[14] Motoya K, Kubota S and Nakaguchi K 1999 *J. Phys. Soc. Japan* **68** 2351
[15] Kaczorowski D, Noel H, Potel M and Zigmunt A 1994 *J. Phys. Chem. Solids* **55** 1363
[16] Kawakami M 1993 *J. Magn. Magn. Mater.* **128** 284
[17] Franse J J M 1977 *Physica* B **86–8** 283
[18] Gratz E and Lindbaum A 1994 *J. Magn. Magn. Mater.* **137** 115
[19] Ueda K and Moriya T 1975 *J. Phys. Soc. Japan* **39** 605
[20] Nishino Y, Kato M, Asano S, Soda K, Hayasaki M and Mizutani U 1997 *Phys. Rev. Lett.* **79** 1909
[21] Sakurai J, Yamamoto Y and Komura Y 1988 *J. Phys. Soc. Japan* **57** 24
[22] Ziman M 1960 *Electrons and Phonons* (London: Oxford University Press)